Meteorol. Z. (Contrib. Atm. Sci.), Vol. **29**, No. 2, 97–116 (published online March 17, 2020)

UTCI climatology and its future change in Germany – an RCM ensemble approach

Benedict Manuel Brecht[1,3*], Gerd Schädler[1] and Janus Willem Schipper[1,2]

[1]Institute of Meteorology and Climate Research, Karlsruhe Institute of Technology, Germany
[2]South German Climate Office at Karlsruhe Institute of Technology, Germany
[3]Current affiliation: Lohmeyer Consulting Engineers, Karlsruhe, Germany

(Manuscript received November 28, 2019; in revised form February 7, 2020; accepted February 12, 2020)

Abstract

In the present study, the quantity, duration and intensity of heat stress events in Germany as well as their future change and relation with weather types were investigated. A small ensemble of regional climate simulations with the regional climate model (RCM) COSMO-CLM driven by four general circulation models (GCMs) was used to calculate the Universal Thermal Climate Index (UTCI); the UTCI is a well-accepted thermal comfort index which we use here to quantify thermal stress. The variables entering the UTCI were bias corrected with a method that preserves their interdependencies. The projected climate changes cause a significant increase of both the mean UTCI and the number, duration and intensity of heat stress events between the control period (1981–2000) and the projection period (2031–2050). The projected future hourly frequency distribution of the UTCI at a location can be described by a shift to higher UTCI values with an almost constant shape of distribution. The investigations of the projected changes in weather types show no significant changes between the periods covered, with a few exceptions. An exception concerning heat stress events is the increase of summer anticyclonic weather types. Although more anticyclonic weather types in summer lead to an increase in heat stress events, they are not the primary cause of the projected increases. Rather, it turns out that the characteristics of the air masses associated with the weather types change towards warmer and more humid conditions.

Keywords: heat stress, UTCI, COSMO-CLM, climate ensemble, multivariate bias correction, climate change

1 Introduction

The mid-latitudes were affected by several severe and long lasting heat waves during the last decades. For example, during the dry and hot summer in Western Europe 2003 (Fouillet et al., 2006; Schär and Jendritzky, 2004) and the extreme heat wave in Russia in June 2010 (Matsueda, 2011), heat induced death tolls are estimated up to 70 000 (Robine et al., 2008) and 20 000 (Revich and Shaposhnikov, 2012), respectively. More recently, an extremely long dry and hot period hit Central and Northern Europe in 2018 (Albergel et al., 2019; Kornhuber et al., 2019).

In a warming world, the likelihood of extreme heat waves increases, affecting 9 % of the world population (700 million people) at an increase of the global mean air temperature by 1.5 °C and almost one-third of the world population (2 billion people) by 2 °C (Dosio and Fischer, 2018). With a global mean air temperature rise of 2 °C, Europe will experience higher warming compared to the global average (Vautard et al., 2014). Also, the likelihood of an event like the heat wave 2003 has doubled in Europe (Stott et al., 2004), increasing the risk of heat-related mortality (Mitchell et al., 2016).

An additional aspect during many heatwaves, which increase the health impact on humans, is the increase of absolute humidity. Already Haldane (1905) points out the relationship between human comfort and air humidity. High humidity leads to a reduced ability of the human body to release heat, which occurs at high temperature mainly through the production of sweat on the skin. With increasing humidity, the evaporation rate decreases and reduces the efficiency of the human cooling system at high temperature. Thus, the combination of heat and high humidity presents a major hazard, even if temperature are not that extreme.

One measure for the combination of temperature and air humidity is the wet-bulb temperature. If the wet-bulb temperature exceeds around 35 °C, the natural cooling effect does not work anymore, leading to hypothermia and, if not counteracted sufficiently, eventually to death (Im et al., 2017; Schär, 2016; Sherwood and Huber, 2010). However, using the wet-bulb temperature as the sole indicator for thermal comfort of humans in relation to thermal stress under warm and humid conditions overestimates the impact of humidity (Vernon and Warner, 1932; Gagge et al., 1986; Jendritzky et al., 1990), as the human well-being, in the context of ther-

*Corresponding author: Benedict Manuel Brecht, Lohmeyer Consulting Engineers, Germany, e-mail: benedict.brecht@lohmeyer.de

mal comfort, depends on more influencing factors than just those two. In terms of thermal environmental parameters, these are air temperature, mean radiant temperature, humidity and air movement, and in terms of behavior, metabolic rate and clothing (Fanger, 1970).

Advanced methods to determine thermal comfort/discomfort are based on heat balance models of the human body. An early assessment of the effect of meteorological variables combined with metabolic rate and clothing led to a general equation describing comfort, which resulted into the Predicted Mean Vote (PMV) index (Fanger, 1970). On the basis of the comfort equation several indices were developed in the following decades, e.g. the "Klima-Michel" model (Jendritzky et al., 1979; Jendritzky et al., 1990), from which the perceived temperature later emerged as a thermal comfort index (Staiger et al., 1997), and the Physiologically Equivalent Temperature index (Mayer and Höppe, 1987; Höppe, 1999). Gagge et al. (1986) refined the PMV-index leading to the PMV*-value (Jendritzky et al., 2007), considering the effect of the enthalpy of sweaty skin and humid clothing. However, all of these indices have deficiencies with regard to thermoregulation processes and heat exchange (Jendritzky et al., 2009). Up to now, those indices have been applied to short episodes of a few days due to the lack of field studies of longer duration. In this work, we want to apply the UTCI on climatological time scales in order to obtain change signals of UTCI statistics.

In the present study, we choose the Universal Thermal Climate Index (UTCI) as a thermal stress indicator; it takes the thermal environmental parameters mentioned above into account (Jendritzky et al., 2012) and employs an advanced thermo-physiological model (Pappenberger et al., 2015). In contrast to the mentioned advanced indices, the UTCI uses the wind speed at a height of 10 m above ground level, making it well suited for operational data and applications at spatial scales from city quarters onwards, whereas indices using the wind speed at the biometeorological reference height of 1.1 m above ground level are more suitable for building and street resolving simulations. The UTCI is the result of multidisciplinary work in the fields of thermal physiology, medicine, meteorology, modelling and software development (Blazejczyk et al., 2012). It combines a thermal comfort model with a clothing/metabolism model focusing on urban population (e.g. Bröde et al., 2012; Fiala et al., 2010; Fiala et al., 2012; Havenith et al., 2012) and is, like the windchill factor, an equivalent temperature. The UTCI has been successfully tested as an index for capturing the bioclimatic variability within Europe (Di Napoli et al., 2018) as well as in probabilistic forecasts on a global scale for international health-hazard warnings and disaster preparedness (Pappenberger et al., 2015) and for the projection of the climate change in Hong Kong on the basis of three GCMs (Cheung and Hart, 2014).

Longer-lasting heat periods, such as the 2003 heat wave in Western Europe, will occur more frequently in the future (e.g. Stott et al., 2004; IPCC, 2013; Lau and Nath, 2014). Recent studies link the occurrence of heat waves in Europe to large scale wave structures in the upper troposphere and/or lower stratosphere which enhances atmospheric blocking over Central Europe (e.g. Fragkoulidis et al., 2018; Lau and Nath, 2014; Schubert et al., 2011). Such events are determined by the large-scale weather, which in our case means throughout Europe, over a longer period of time, i.e. a few weeks to months. The current synoptic conditions can modify the large-scale weather character for a few days. It is therefore important to understand the impact of weather types on the UTCI in a changing climate and their connections with heat stress events. This will be studied in this paper using the objective weather type classification of the German Weather Service (DWD; Dittmann et al., 1995; Bissolli and Dittmann, 2001). For Central Europe, it is expected that within the general warming of the continent throughout the year, the air temperature differences between colder and warmer weather situations stay constant and the summertime anticyclonic weather situations will become more frequent (Riediger and Gratzki, 2014; Chang et al., 2016).

Due to their coarse spatial resolution, GCMs are not able to capture regional details. Therefore, GCMs are downscaled statistically or dynamically on a finer grid within an area of interest (e.g. Schädler et al., 2018). With regard to dynamical downscaling the so-called Regional Climate Models (RCMs) are an important tool to study regional climate impacts as well as to develop climate adaptation strategies (Rummukainen, 2010; Hackenbruch et al., 2016; Hackenbruch et al., 2017; Schipper et al., 2019).

One focus of the present study is the change of the UTCI in Germany, especially with respect to heat stress, between the control time period (1981–2000) and the projection time period (2031–2050). The other focus is on the relation between weather types and UTCI and the effect of possible changes in weather types and their properties on the UTCI between the control and the projection time period.

Using an ensemble of regional climate simulations created with COSMO-CLM (Rockel et al., 2008), which are based on the driving data of various global models, the effects of future climate changes on heat stress events are calculated for Germany using the UTCI. In order to calculate UTCI thresholds, for the first time, a bias correction based on seasonal hourly values with the multivariate bias correction for climate model projections of several climate variables, MBCn (MBC N-pdft, Multivariate Bias Correction N-dimensional probability density function transform) (Cannon, 2017; Brecht, 2019) was performed.

Section 2 describes the data and method used to build the UTCI as well as the bias correction. Section 3.1 describes the UTCI change signal in Germany, followed by a study of the connection between changes of the weather types and the UTCI in Section 3.2. Finally, Section 4 contains the conclusion.

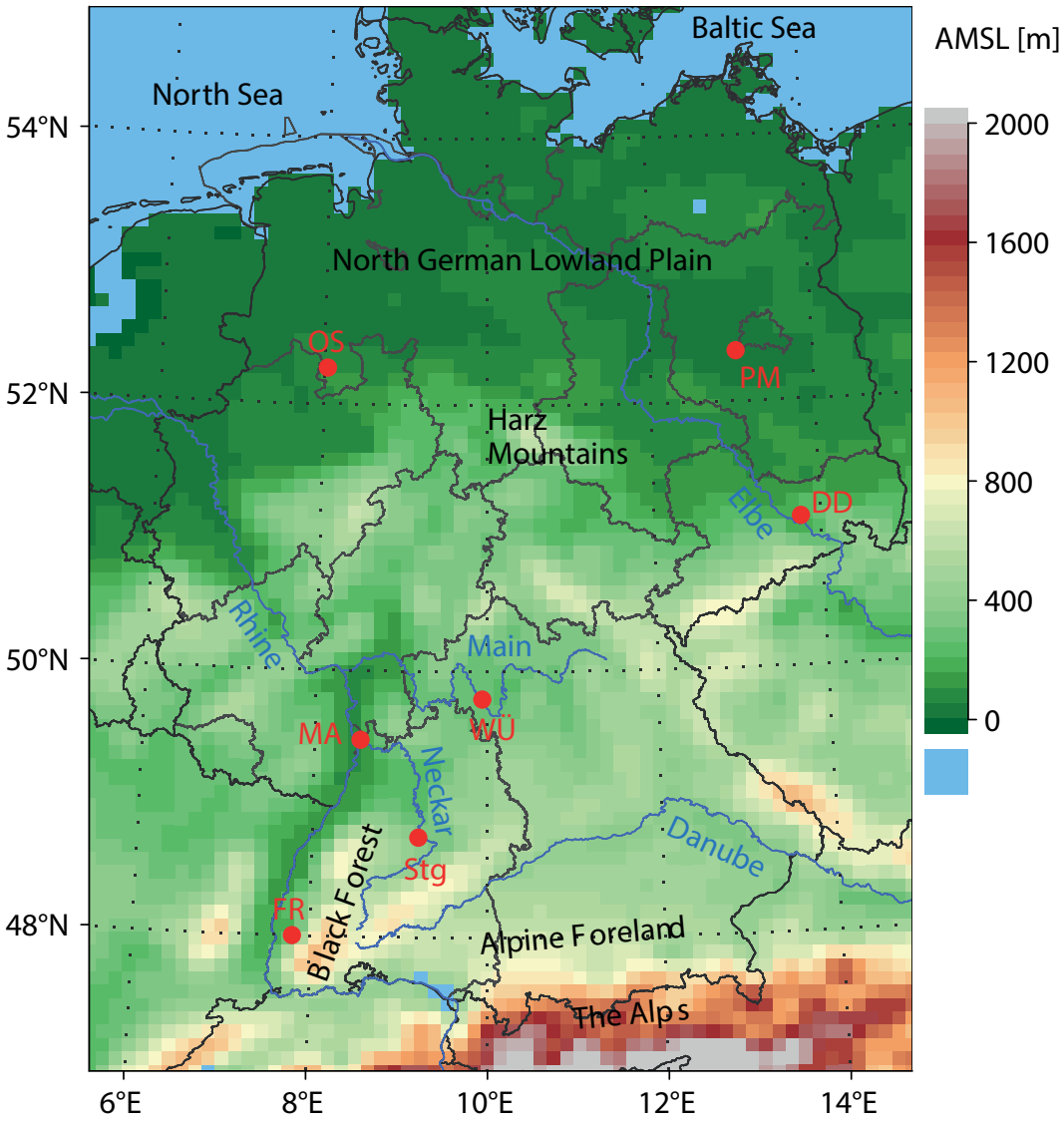

Figure 1: Investigation area and neighbouring countries. The red dots show the locations of the SYNOP stations Osnabrück (OS), Potsdam (PM), Dresden (DD), Würzburg (WÜ), Mannheim (MA), Stuttgart (Stg), and Freiburg (FR) described in Section 2.4.

2 Methods and data

2.1 Investigation Area

The investigation area is Germany. Figure 1 shows the relief of Germany and parts of neighbouring countries in the mesh width used in this study. From the wide spectrum of orographical features result a wide range of UTCI values and change signals including regions experiencing heat stess already like the Rhine valley, the Bight of Cologne and parts of Eastern Germany. To the very south of Germany are the Alps and the Alpine Foreland. This is followed by a large area with complex terrain including the Black Forest, the Swabian Alb, the Ore Mountains and the Harz Mountains. The area also includes the warm low-lying valleys of the Rhine, Neckar, Main and Danube catchments and their tributaries as well as densely populated metropolitan regions like the Rhine-Main area, the Rhine-Neckar area, and the Munich and Stuttgart metropolitan areas. North of the low mountain range the North German lowlands are found, which include the warm parts along the Lower Rhine with the Ruhr area in the west and the summerly warm and dry parts of Brandenburg, Berlin and Northern Saxony in the east.

2.2 The Regional Climate Model COSMO-CLM

For our simulations we used the RCM of the Consortium for Small-scale Modeling in Climate Mode, COSMO-CLM (CCLM), model version cosmo_090213_4.8_clm17. It is based on the operational weather forecast model COSMO of the DWD and is described in Steppeler et al. (2003). CCLM is a non-hydrostatic model based on the primitive thermo-hydrodynamical equations describing compressible flow in a moist atmosphere. It uses a rotated lon-lat-grid with the equator

and the prime meridian near the center of the modeling domain. In the vertical, a generalized terrain following height coordinate is used. For the grid structure in CCLM a horizontally uniform, 3-dimensional Arakawa-C/Lorenz grid is used (Lorenz, 1960; Harlow and Welch, 1965; Arakawa and Lamb, 1977). The temporal integration is done by a third-order Runge-Kutta method (Liu et al., 1994; Wicker and Skamarock, 2002). Subgrid scale processes are described by various parameterization schemes (Doms et al., 2011). CCLM provides four schemes for the parameterization of precipitation, which differ in the number of hydrometeor types considered. Here a cloud-ice single moment scheme with the variables cloud water content and cloud ice content in addition to the water vapour and the precipitable rain and snow is used. In order to parameterize subgrid-scale deep convection, a mass flux scheme according to Tiedtke (1989) is used in CCLM. For shallow convection, a reduced scheme according to Tiedtke (1989) is used. Climatologies are used for the content of ozone, carbon dioxide and aerosols in the different layers. Subgrid-scale orography is parameterized according to Lott and Miller (1997). A detailed description of CCLM can be found in Rockel et al. (2008). Lower boundary conditions for the atmospheric model were provided by the soil vegetation atmosphere transfer scheme (SVAT) TERRA_ML, which is the SVAT implemented by default in CCLM. TERRA_ML is a multilayer (including snow) SVAT based on the two-layer TERRA developed by Jacobsen and Heise (1982). Soil temperature is calculated by solving the heat diffusion equation with moisture dependent heat capacity and heat conductivity, whereas soil moisture is calculated using the Richards equation with moisture dependent hydraulic diffusivity and conductivity. Coupling with the atmosphere is done via moisture (precipitation, evapotranspiration) and energy fluxes (ground heat flux). Vegetation is accounted for via time dependent plant cover and leaf area index. In the soil, ten layers down to about 17 m depth are used.

2.3 The Regional Climate Simulations Ensemble

The regional climate ensemble used here consists of four CCLM simulations driven by four GCMs; additionally, a validation run driven by ERA-Interim (Dee et al., 2011) was performed. The GCM driven simulations for the control period 1981–2000 and the projection period 2031–2050 with emission scenario RCP 8.5 are subset of the ones described and performed by Sedlmeier (2015) respectively Sedlmeier et al. (2017). For spin-up, the simulations were started three years before the respective time period. Since the difference between the resolution of the driving GCMs (about 200 km) and the target resolution of 0.0625° (about 7 km) is large, a double nesting procedure was used with a coarse nest at 0.44° (about 50 km) resolution and a fine nest at 0.0625° resolution; Figure 2 shows the domains with the corresponding mesh sizes. The 7 km model domain has 165×200 horizontal grid points and 40 non-equidistant vertical layers. After initializing the atmospheric and soil fields, only the atmospheric boundary conditions are updated every six hours. An overview of the GCMs used is given in Table 1.

2.4 Observation data

Two kinds of data sets were used for model validation.

For area-wide comparisons at a daily temporal resolution, we used the HYRAS data set (Rauthe et al., 2013; Frick et al., 2014). This gridded data set was developed by the DWD and contain daily values of air temperature, relative humidity and precipitation at a resolution of 5 km by 5 km for a region covering the major river catchments in Central Europe; it is based on station observations and advanced interpolation methods for the period 1951–2006. The model evaluation was performed with regard to the UTCI related variables air humidity and air temperature on the basis of mean values of the individual seasons.

In addition to the variables air temperature and humidity, the other variables entering the UTCI, wind speed and radiation, and finally also the UTCI were compared with observations. For that purpose station data from observation sites of the DWD (so-called SYNOP Data) were used. The sites were selected according to the following criteria:

- all data necessary to calculate the UTCI are available, namely: air temperature and relative humidity at 2 m height, cloud cover, direct and diffuse radiation and wind speed at 10 m height.
- the time series cover the period 1981–2000 (validation of control period) and/or 1995–2012 (validation of bias correction, see below).
- the stations are situated in different regions of Germany in order to be representative.

These conditions were fulfilled at least partially by eight stations whose locations are shown in Figure 1 by red dots. With the station data, in addition to the mean values of the seasons, mean daily cycles, probability distributions and threshold values of the UTCI and the parameters entering it were analysed. The station data are freely available at the Climate Data Center (CDC) of the DWD. A brief description of the model evaluation with the described data is given in Section 2.6.2.

2.5 UTCI

As a quantitative measure for human thermal comfort or discomfort (i.e. cold or heat stress), we use the Universal Thermal Climate Index UTCI (Jendritzky et al., 2012). We give only a brief description here, details can be found e.g. in Jendritzky et al. (2012), Bröde et al. (2012), Fiala et al. (2010); Fiala et al. (2012), and Havenith et al. (2012). The UTCI is the result of mul-

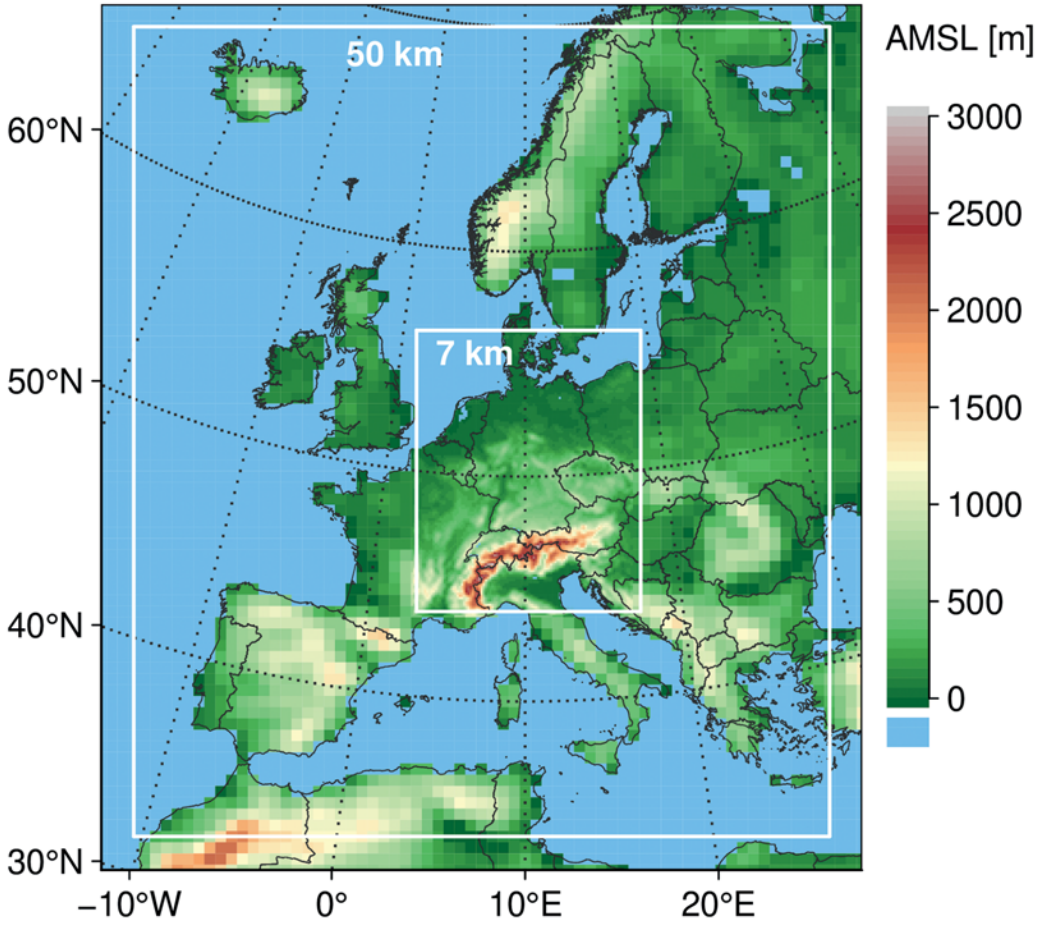

Figure 2: Computational domains of the CCLM simulations used with the corresponding mesh sizes.

Table 1: GCMs and reanalysis data used as initial and boundary data for the CCLM Ensemble.

Name	Atmospheric model	Institute	Emission scenario	Resolution (atmosphere)	Reference
ECHAM6	MPI-ESM-LR	Max Planck Institute for Meteorology, Germany	RCP8.5	1.8°	Stevens et al. (2013)
EC-EARTH	EC-EARTH	EC-EARTH Consortium, Europe	RCP8.5	1.125°	Hazeleger et al. (2012)
CNRM-CM5	CNRM-CM5	National Centre for Meteorological Research, France	RCP8.5	1.4°	Voldoire et al. (2013)
Hadley	HadGEM2-ES	Met Office Hadley Centre, UK	RCP8.5	1.25° × 1.875°	Collins et al. (2011)
ERA-Interim	IFS	ECMWF, UK	Reanalysis	1.125°	Dee et al. (2011)

tidisciplinary work in the fields of thermal physiology, medicine, meteorology, modeling and software development. It combines a thermal comfort model with a clothing/metabolism model focusing on urban population (McGregor, 2012). Quantitatively, the UTCI is an equivalent temperature which gives for a combination of air temperature, wind, radiation and humidity the equivalent air temperature of a reference condition that would produce the same response of the physiological model. The UTCI temperature can be categorized in terms of thermal stress according to the UTCI standard assessment scale shown in Table 2. It should be noted that human adaptation and acclimatisation to heat is not taken into account there, so that it can be seen more as an aid to assess whether temperature thresholds of the UTCI have been reached or exceeded. The reference condition is defined as an environment with a wind speed of 0.5 m s^{-1} at 10 m height, a mean radiant temperature equal to the ambient air temperature, a vapour pressure which corresponds to a relative humidity of 50 %, but having a maximum value of 20 hPa (Bröde et al., 2012). It is furthermore assumed that persons have a metabolic rate of 2.3 MET (corresponding to a walking speed of 1.1 m s^{-1}) and wearing clothing with a thermal resis-

Table 2: Thermal stress levels and associated value range of the UTCI for the UTCI standard assessment scale according to Bröde et al. (2012).

Thermal stress level	UTCI in °C
Extreme heat stress	> 46
Very strong heat stress	38 to 46
Strong heat stress	32 to 38
Moderate heat stress	26 to 32
"Thermal comfort zone"	18 to 26
No thermal stress	9 to 18
Slight cold stress	0 to 9
Moderate cold stress	−13 to 0
Strong cold stress	−27 to −13
Very strong cold stress	−40 to −27
Extreme cold stress	< −40

tance modeled by the UTCI-clothing model (Havenith et al., 2012). The model uses the UTCI-Fiala model (Fiala et al., 2012) as its thermoregulation model which models an average person with a weight of 73.4 kg and a surface body area of 1.85 m^2. Also included is a model to predict thermoregulatory reactions of the central nervous system, e.g. shivering or sweating. In general the UTCI increases with air temperature, radiant temperature and water vapour pressure. With increased wind speed the UTCI decreases, unless the ambient temperature is above core temperature.

In its original form, the model is computationally expensive and therefore not suitable for large numbers of simulations as required in this study. Therefore, Bröde et al. (2012) proposed two methods for approximating the UTCI: a look-up table of pre-calculated UTCI values (about 2 orders of magnitude faster) and a 6th order regression function (about 5 orders of magnitude faster). Clearly, the regression function is most commonly used; we also used it in this study. The function is only valid within certain bounds (ambient air temperature between −50 °C and +50 °C, mean radiant temperature: 50 °C below and 70 °C above air temperature, wind speed at 10 m height between 0.5 m s^{-1} and 17 m s^{-1}, vapour pressure between 0 hPa and 45 hPa (Bröde et al., 2012), which were never attained in our study. The quantities are normally considered at the biometeorological reference height 1.1 m above ground level. However, since climate model data and measurement data are normally output at a height of 2 m, except for wind speed at 10 m height, the values of the variables at 2 m height above ground were used throughout this study. This may lead to a minor underestimation of the absolute values of the UTCI on low-wind and sunny days and a minor overestimation on low-wind and cloudless nights, but does not change the projected development of the UTCI.

2.6 Bias correction

Climate simulations of numerical models often have systematic deviations from the values observed in reality, which limits their applicability in climate impact models (Maraun, 2013); therefore, so-called bias corrections are often applied. In many cases, quantile mapping (QM) is used as a bias correction method (Vrac et al., 2016). Since modern thermal indices such as the UTCI are composed of several variables, QM, which is applied to every variable separately is not sufficient for bias correction because the relationships between the meteorological variables forming these indices are not taken into account; this is also to a large extent true for most multivariate bias-correction methods (e.g. Bürger et al., 2011; Vrac and Friederichs, 2015; Cannon, 2016), which consider the relationships between variables to a limited extent only (Cannon, 2017). Hence, in the following the state-of-the-art MBCn bias correction algorithm by Cannon (2017) is used.

2.6.1 Method

The MBCn adapts an image processing technique – the N-dimensional probability density function transform (N-pdft) – that is designed to transfer color information from one image to another to make the target image look like the original image. With modifications the technique can be used to correct several climate variables simultaneously without losing their interdependencies and by preserving their climate change signal. Therefore matrices of the source data (historial climate simulations), projection data (climate projections) and the target data (observed data) are required, with the variables arranged as columns and the points in time as rows. First an orthogonal rotation is applied to the data sets, which produce linear combinations of the original variables; in the second step, univariate quantile delta mapping (QDM; Cannon, 2016) is applied to these. The QDM transfer function is used so that the absolute changes, e.g. for the temperature, respectively relative changes, e.g. for the wind speed, are preserved in the quantiles. In the third step an inverse rotation is applied to the resulting data to obtain the source values for the next iteration step. To preserve the ratio property of variables like wind speed in the first step, a fourth step is added, where the corresponding absolute/ratio version of QDM is applied to each variable of the original projection data using the source data and target data as baseline data. Then the quantiles of each column of the third step with respect to the projection data are replaced with those from the obtained in the application of QDM from the fourth step. The four steps are repeated iteratively until the multivariate distribution matches the target distribution. A more detailed description can be obtained from Cannon (2017). The MBCn algorithm is available as a package ("MBC") of the free programming language for statistical calculations and graphics R and was used for this study. A documentation can be found at https://cran.r-project.org/web/packages/MBC/MBC.pdf.

In addition to selecting the method for bias correction, adequate observation data are also required. Hourly observations of the variables forming the UTCI – air temperature, direct and diffuse short-wave irradiation,

wind speed, humidity and cloud cover – are necessary for the calibration period, but are rarely available in this form in a spatially covering grid. Gridded data with the necessary parameters in hourly temporal resolution are available for the time period 1995–2012 from the test reference years (TRY) data set which is freely available from the DWD CDC (ftp://opendata.dwd.de/climate_environment/CDC/; last called 27 November 2019) and has a spatial resolution of about 1 km. Among other quantities, the required variables air temperature, cloud cover, humidity, direct and global radiation as well as wind speed are available. The data are based on station data, satellite observations and model data, which are extrapolated to the grid with a raster method adapted to the respective variable. For each variable, a quality estimate with hints for the application is provided. More details on the data can be found in Krähenmann et al. (2018). For the present study, we interpolate the TRY data to the mesh width of the climate simulations and validate them with the observational data sets mentioned in Section 2.4. The validation of the data is described in Brecht (2019).

For the bias correction, hourly observations (TRY) are only available for the period 1995–2012, whereas the control period of the simulation ensemble is 1981–2000. Therefore, the bias correction, using the MBCn method, is performed in two steps. First, an ERA-Interim driven CCLM run which is available from 1981–2012 is used with the TRY data as observational data to obtain bias correction factors for the overlap period 1995–2012. These factors are then used to calculate a bias corrected ERA-Interim driven CCLM run (called reference run) for the control period 1981–2000. In detail this means that with the variables as columns and the points in time as rows matrices were formed for the TRY data (observations, 1995–2012), and ERA-Interim driven CCLM data (1981–1996 and 1997–2012, to have data sets of the same length). The matrices were produced separately for each grid point as well as for each hour of day and season and were inserted into the MBCn algorithm. As result, MBCn outputs the corrected variables for 1981–1996 and 1997–2012, which were reassembled in time and spatially. The years 1981–1996 and 1997–2000 are cut out of the data sets and merged as the new reference data set. The variables used for the MBCn algorithmus were the air temperature, air humidity, surface pressure, global radiation, ratio of diffuse radiation, horizontal wind components and cloud cover. In the second step each CCLM climate ensemble run is separately bias corrected with the reference run for the control period 1981–2000 and the projection period 2031–2050. The detailed procedure is the same as in the first step, with the three data sets now being the reference data set formed in step 1, the historical climate simulations and the climate projections.

2.6.2 Results

First, a brief description of the model validation against the observational data mentioned in Section 2.4 is given. The comparison of CCLM simulations driven by ERA-Interim and HYRAS show that CCLM is able to reproduce the observations on the area quite well. The simulations driven by the four GCMs show significant negative deviations from HYRAS over the whole area with respect to air temperature in all seasons, except for the simulations driven by Hadley during summer and the simulation driven by ECHAM6 in autumn and winter; for relative humidity it is the other way round. Concerning the station data, comparisons of ERA-Interim driven CCLM simulations show that CCLM is capable of modeling the UTCI and the variables entering the UTCI realistically. The characteristics of individual SYNOPs also show that local effects can influence the UTCI, such as local mountain wind systems, which cannot be reproduced by CCLM with the mesh size of 7 km. For the UTCI, comparisons of CCLM simulations driven by the GCMs show that, as for air temperature on the area, the mean values of the UTCI are significantly underestimated, with the underestimation being larger during the day than at night and larger in summer than in winter. Overall, this leads to a significant underestimation of the occurrence of hours during which heat stress occurs, since this occurs mainly during the summer half-year and during the day. A more detailed description of the validation of the simulations against the observations is discussed in Brecht (2019).

The Tables 3 and 4 show the mean errors of the UTCI and the variables entering it from the simulations driven by ERA-Interim and the GCMs compared to the observational data from the Mannheim station. The Mannheim station is taken as an example; the qualitative results of the differences between the simulations and observations are also valid for the other mentioned stations, although the results are not identical due to regional and local characteristics. For the ensemble mean of the GCM driven CCLM simulations the air temperature is underestimated by about 2 K (night) to 2.5 K (day) in winter and by about 1.5 K (night) to 4 K (day) in summer. The global radiation and cloud cover is in good agreement with the observations in winter, whereas in summer it is underestimated respectively overestimated. From the air temperature and radiation as well as cloud cover it follows that the radiant temperature is underestimated in winter by about 1 K (night) to 1.5 K (day) and summer by about 0.5 K (night) and 6.5 K (day). The wind speed is in good agreement with the observations in winter and is underestimated in summer by about 0.5 m s^{-1}. The relative humidity is overestimated in winter by about 4 % (night) to 9 % (day), inverse following the underestimation of the air temperature. In summer the ensemble mean overestimates the relative humidity by about 6 % (night) to 15 % (day). The ensemble mean underestimates the vapour pressure by nearly 0.5 hPa in winter and overestimates respectively underestimates it slighlty in summer at day respectively night. The bias corrected values of the described variables compared to the observational data of the Mannheim station is shown in Table 5. Almost all

Table 3: Mean error of the CCLM simulations driven by ERA-Interim to the observational data of the station Mannheim during the control period in winter (DJF) and summer (JJA).

	winter		summer	
	day	night	day	night
Air temperature	−1.4 K	−0.5 K	−1.5 K	0.4 K
Cloud cover	5 %	3 %	11 %	12 %
Diffuse radiation	1 W m^{-2}	–	−24 W m^{-2}	–
Direct radiation	6 W m^{-2}	–	−7 W m^{-2}	–
Radiant temperature	−0.2 K	0.2 K	−2.2 K	1.5 K
Relative humidity	7.5 %	4.4 %	5.9 %	−2.2 %
UTCI	−0.5 K	−0.1 K	−1.5 K	0.4 K
Vapour pressure	0.0 hPa	0.1 hPa	0.4 hPa	0.0 hPa
Wind speed	−0.2 m s^{-1}	−0.1 m s^{-1}	−0.1 m s^{-1}	0.2 m s^{-1}

Table 4: Mean error of the ensemble mean of the CCLM simulations driven by the GCMs to the observational data of the station Mannheim during the control period in winter (DJF) and summer (JJA).

	winter		summer	
	day	night	day	night
Air temperature	−2.6 K	−1.7 K	−3.9 K	−1.6 K
Cloud cover	6 %	5 %	11 %	17 %
Diffuse radiation	10 W m^{-2}	–	−38 W m^{-2}	–
Direct radiation	9 W m^{-2}	–	−47 W m^{-2}	–
Radiant temperature	−1.6 K	−1.1 K	−6.5 K	−0.5 K
Relative humidity	8.4 %	4.2 %	14.8 %	5.8 %
UTCI	−4.3 K	−3.4 K	−4.9 K	−2.3 K
Vapour pressure	−0.4 hPa	−0.4 hPa	0.2 hPa	−0.3 hPa
Wind speed	−0.1 m s^{-1}	−0.2 m s^{-1}	−0.7 m s^{-1}	−0.5 m s^{-1}

Table 5: Mean error of the bias corrected ensemble mean of the CCLM simulations driven by the GCMs to the observational data of the station Mannheim during the control period in winter (DJF) and summer (JJA).

	winter		summer	
	day	night	day	night
Air temperature	−0.2 K	−0.4 K	−0.4 K	−0.3 K
Cloud cover	−4 %	0 %	−3 %	−1 %
Diffuse radiation	1 W m^{-2}	–	−1 W m^{-2}	–
Direct radiation	6 W m^{-2}	–	6 W m^{-2}	–
Radiant temperature	1.9 K	0.2 K	1.4 K	0.8 K
Relative humidity	0.5 %	−0.6 %	0.4 %	−2.0 %
UTCI	0.1 K	−0.3 K	−0.1 K	−0.1 K
Vapour pressure	−0.1 hPa	−0.2 hPa	−0.3 hPa	−0.7 hPa
Wind speed	0.1 m s^{-1}	0.0 m s^{-1}	0.2 m s^{-1}	0.0 m s^{-1}

variables show reduced mean errors after bias correction or remain at a similar level if the error was already small before. Figure 3 shows the corresponding mean daily cycle of the UTCI derived from the simulation ensemble and from observations of the synoptic station Mannheim (MA in Figure 1) in winter (DJF) and summer (JJA). The colored dotted curves show the UTCI of each ensemble member driven with the mentioned GCMs. The red dotted curves show the bias corrected values of the UTCI, which are pretty close together; this results from the daytime-dependent (hourly) bias correction, which means that the average daily cycle of all corrected ensemble members is almost identical. The black line shows the mean daily cyle of the observations at the station Mannheim. The uncorrected UTCI is underestimated by all four CCLM simulations driven by the described GCMs compared to the observations in winter and summer. Only the CCLM simulations driven by ECHAM6 (winter at night) and Hadley (summer) do not highly underestimate the UTCI. The systematic deviations up to 8 K depend on the season and are larger during the day than at night in summer; using the uncorrected UTCI would therefore lead to large underestimates of heat stress. The main reason for the underestimation of the UTCI in the ensemble mean is the low air temperature level described; in combination with too much simulated cloud cover respectively less radiation, the radiant temperature during the day is also significantly underestimated especially in summer. With the hourly and seasonal use of the multivariate bias correction method MBCn, the mean errors are significantly reduced (red dotted curves, differ only marginally) and lead to reliable results on the number of heat stress events.

2.7 Objective weather type classification

To obtain the weather type distribution over Central Europe used in Section 3.2, we used the objective weather type classification after Bissolli and Dittmann (2001). It differentiates between 40 possible weather types which are defined by the combination of three meteorological criteria:

- the advection AA of air masses which can be XX (undefined), NE (northeasterly flow), SE (southeasterly flow), SW (southwesterly flow) or NW (northwesterly flow), based on the zonal and meridional wind components at 700 hPa. If more than two thirds of the grid points show a wind direction in the same sector, this is considered as the predominant wind direction, otherwise the wind direction is defined as XX (no prevailing wind direction),
- the cyclonalities C950 near the surface at 950 hPa and C500 in the mid-troposphere at 500 hPa (C or A), and
- the precipitable water content PW of a tropospheric air column, which can be wet (W) or dry (D); it is calculated from pressure and specific humidity at the 950, 850, 700, 500 and 300 hPa levels. Wet or dry conditions are classified by checking whether the area mean of PW is above (wet) or below (dry) a long term average (July 1979–December 1996) for a given month.

The weather types depending on these criteria are then written as a five-element string AAC950C500PW.

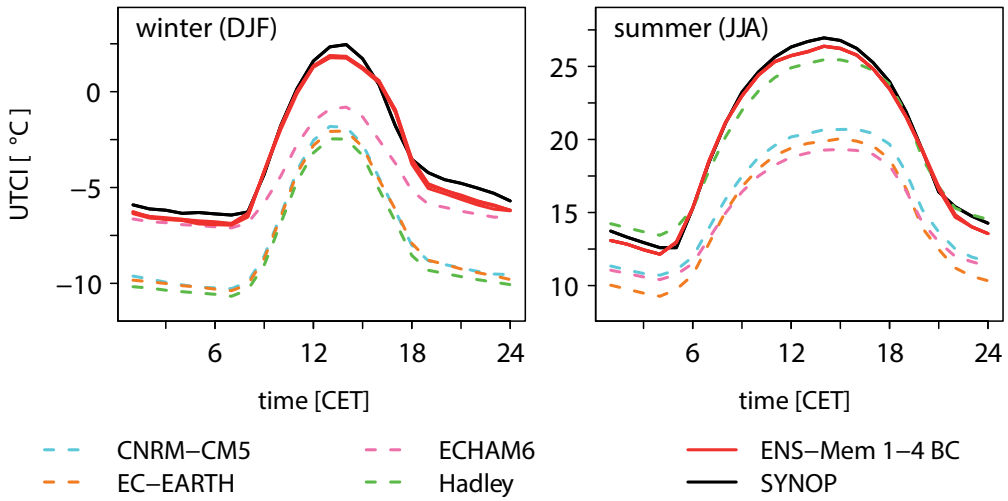

Figure 3: Mean daily cycle of the UTCI derived from the simulation results and observational data of the Mannheim station for winter and summer. The colored dotted curves show the data of the direct model output of each ensemble member of the climate simulations. The red curves show the bias-corrected daily cycles (ENS-Mem 1–4 BC, differ only marginally), and the black curve shows the daily cycle of the UTCI calculated from the station data.

2.8 Metrics used

For comparisons of model simulations with observations, the mean absolute error, the mean error and the standard deviation are used.

To discuss ensembles, we use boxplots containing the mean, the median, the upper and the lower quartile as well as the 5 % and the 95 % quantile. The agreement between ensemble members with respect to a climate change signal of a variable is assessed via the concept of ensemble consistency (EC; Feldmann et al., 2013; Sedlmeier, 2015). That is, EC is the percentage of ensemble members that project a positive/negative change for a variable. Since our ensemble consists of only four members, EC can only take on the nine values ±100 %, ±75 %, ±50 %, ±25 %, 0 %. If more than 66 % of the simulations of an ensemble agree in the direction of the changes, these are considered "likely", more than 90 % are referred to as "very likely" following IPCC (2014). For ensemble agreement, |EC| should be greater than 66 % here, i.e. ±100 % or ±75 %.

The significance of the deviations of the climate simulations from the reference values as well as the significance of projected climate changes are determined with the Wilcoxon rank sum test with a significance level of 95 %.

To compare two data sets relative to a reference data set, we use the Mean Squared Error Skill Score (MSESS), defined as $\mathrm{MSESS} = 1 - \mathrm{MSE}_1/\mathrm{MSE}_2$, where $\mathrm{MSE}_{1,2}$ are the mean squared errors of data set 1 and data set 2, respectively. If data set 1 better reproduces the reference data, the MSESS is positive, otherwise negative.

3 Results

In this section, the projected changes of the UTCI and their relation with the weather types between the control period 1981–2000 and the projection period 2031–2050 are presented. With regard to the 2 °C threshold (e.g. Vautard et al., 2014), the projection period represents the timespan in which the threshold is reached and exceeded by most GMCs under the emission scenario RCP8.5; it is known that regionally, large deviations from the 2 °C value can occur (Vautard et al., 2014). We study how the UTCI in the investigated area behaves when the global 2 °C threshold is reached. We discuss the projected changes of the UTCI with regard to seasonal mean values, exceedance of threshold values, duration of heat stress events and hourly probability distributions (Section 3.1). All results are based on MBCn bias corrected data (Section 2.6). Finally, we look at the connenction between the projected changes of the weather types and those of the UTCI (Section 3.2).

3.1 UTCI changes

First, the mean changes of the variables entering the UTCI are briefly described (more details in Brecht, 2019). The tables 6 and 7 show the corresponding values of the parameters described below as a spatial mean over Germany for the winter respectively summer. The climate change signal of the air temperature is positive all over Germany throughout the year, ensemble consistent and significant at the 95 % level. The spatially averaged changes between the control and projection period range from 1 K in spring to 1.7 K and 1.8 K in summer and autumn, respectively; the spatial differences of

Table 6: Spatial mean over Germany in the control period (ctrl), difference between projection and control period (proj – ctrl), consistency of the differences across the ensemble (EC) and significance of the differences (Sig) for the UTCI and variables entering it for the winter season (DFJ).

Variable	ctrl	proj – ctrl	EC in %	Sig in %
Air temperature	0.9 °C	1.6 K	100	100.0
Cloud cover	73 %	2 %	80	96.6
Diffuse radiation	24 W m^{-2}	−2 W m^{-2}	−100	100.0
Direct radiation	12 W m^{-2}	−2 W m^{-2}	−97	98.6
Radiant temperature	2.5 °C	1.5 K	100	100.0
Relative humidity	85.7 %	0.6 %	97	95.4
UTCI	−8.0 °C	2.1 K	100	100.0
Vapour pressure	5.9 hPa	0.7 hPa	100	100.0
Wind speed	4.1 m s^{-1}	0.0 m s^{-1}	21	31.0

Table 7: Spatial mean over Germany in the control period (ctrl), difference between projection and control period (proj – ctrl), consistency of the differences across the ensemble (EC) and significance of the differences (Sig) for the UTCI and variables entering it for the summer season (JJA).

Variable	ctrl	proj – ctrl	EC in %	Sig in %
Air temperature	16.9 °C	1.7 K	100	100.0
Cloud cover	59 %	−2 %	−81	98.6
Diffuse radiation	105 W m^{-2}	−2 W m^{-2}	−80	89.2
Direct radiation	96 W m^{-2}	5 W m^{-2}	74	87.2
Radiant temperature	27.9 °C	1.8 K	100	100.0
Relative humidity	73 %	0 %	−56	40.6
UTCI	16.8 °C	2.2 K	100	100.0
Vapour pressure	13.8 hPa	1.4 hPa	100	100.0
Wind speed	3.0 m s^{-1}	−0.1 m s^{-1}	−91	100.0

the changes are very small. This is in accordance with the results in Sedlmeier (2015). With the exception of spring, the change in radiant temperature also has a high EC throughout Germany, significant changes at the 95 % level and a positive change signal between 1.5 K in winter and 1.8 K and 1.9 K respectively in summer and autumn. In spring, the projected changes are slightly lower at 0.6 K. The reason for this is a reduced direct and diffuse solar radiation in spring due to an increased degree of cloud cover. In winter, a higher degree of cloud cover is projected and thus the direct radiation is reduced, but this has less effect on the air temperature due to the lower position of the sun. For summer and autumn, a lower degree of cloud cover and therefore more direct radiation is projected. With regard to wind speed, a significant decrease is projected for summer. For relative humidity, the seasonal change signals are different throughout Germany. A higher relative humidity is projected for winter and spring, which is significant in large parts of Germany in winter and has a high EC. In spring, a significant increase in relative humidity is projected for the lower lying parts of southwest Germany. In summer no significant changes are projected, and in autumn there is a significant decrease of relative humidity in the ensemble, especially in the west and southwest as well as in central Germany. In contrast to the relative humidity, which decreases when the temperature rises and increases when the absolute humidity rises, the vapour pressure increases when the temperature rises and the absolute humidity rises. The climate change signal of the vapour pressure varies in the spatial and temporal average between 0.7 hPa in winter and spring to 1.4 hPa in summer. This corresponds approximately to the changes in saturation vapour pressure that can be expected due to the projected air temperature changes, i.e. the atmosphere can store more water; the higher the air temperature, the greater the increase in saturation vapour pressure per temperature interval (Clausius-Clapeyron law). Since vapour pressure depends on both temperature and humidity, this quantity is very robust to show the climate change that is taking place. EC is 100 % throughout the entire area and significance is given at the 95 % level everywhere (Brecht, 2019).

According to the changes of the single variables, the seasonal mean values for winter and summer of the UTCI in the control and projection period and their differences are shown in Figure 4. The spatial mean value of the UTCI ranges from −8 °C in winter to 16.8 °C in summer, i.e. a greater amplitude of the annual cycle than the ground-level air temperature. Overall, the UTCI in the coastal areas is considerably lower due to maritime influence on wind and air temperature than in the areas farther inland. For the same reasons, i.e. higher wind speed and lower air temperature, the UTCI is also lower in mountainous regions. The Upper Rhine valley and the Rhine-Neckar area are the regions in Germany with the highest UTCI mean values in summer, i.e. 18.5 °C to 20.5 °C. In the Rhine-Main region, along the Rhine valley, along the Danube in south-eastern Bavaria, in northern Saxony, parts of Saxony-Anhalt and Brandenburg, high UTCI mean values are reached in summer as well, i.e. 18 °C to 20 °C; these areas are lower compared to their surroundings, i.e. have a higher average air temperature. In addition, there are higher moisture inputs in the river valleys and a higher continentality in the east and northeast of Germany, which leads to less cloud formation and thus more irradiation and a higher radiant temperature, as for example in the low-lying areas of northwest Germany. For the projection period, the UTCI mean values increase quite uniformly throughout all seasons of the year, while the spatial differences remain. The projected mean future changes of the UTCI are 1.3 K in spring, 2.1 K in winter and autumn and 2.2 K in summer. The EC is 100 % throughout, so it is robust over the entire investigation area, and the changes are significant everywhere at the 95 % level. Note that the projected changes of the UTCI are greater than those of the air temperature in 2 m due to the interaction of temperature and humidity increases.

Concerning the frequency of heat stress events and its change, Figure 5 shows the mean number of days per year on which at least strong (32 °C) and very strong heat stress (38 °C) is reached at least once a day, based

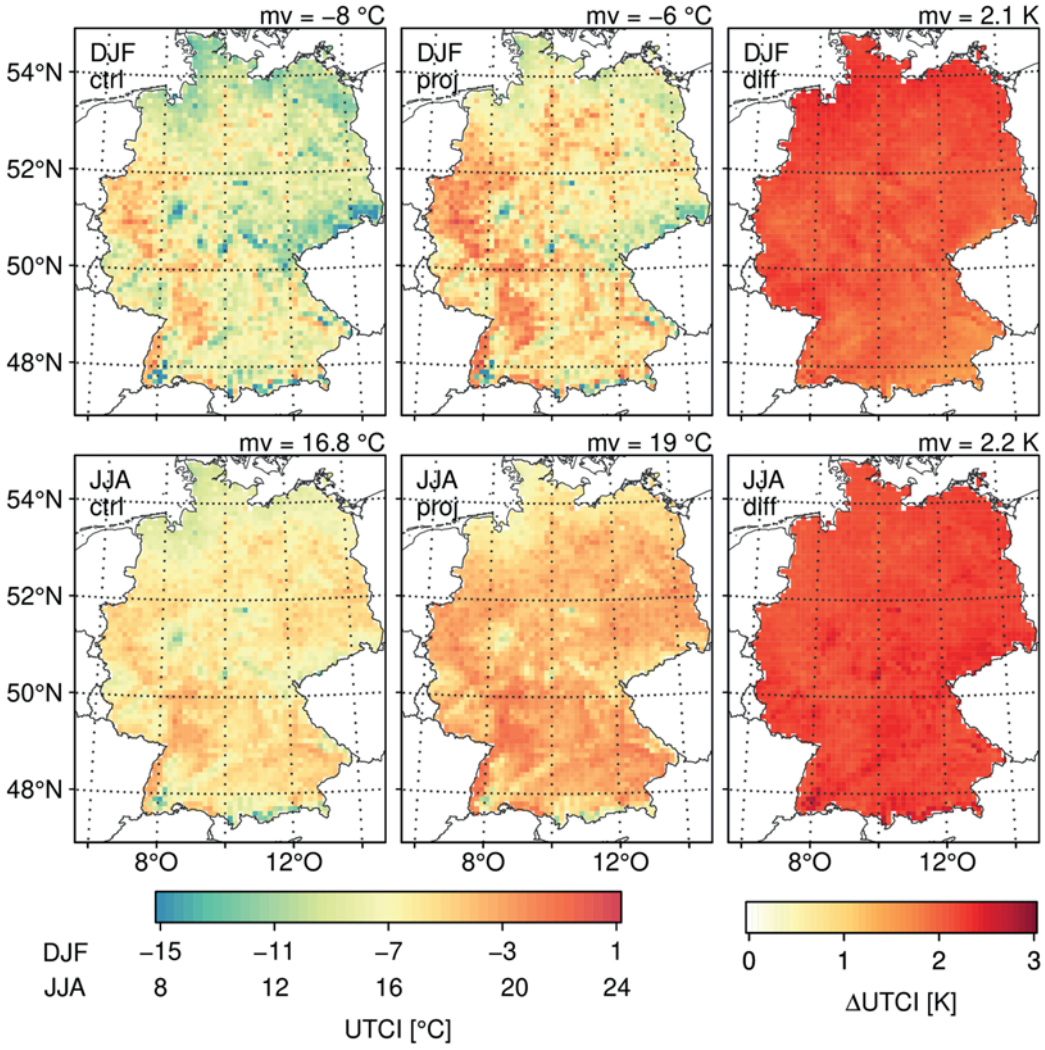

Figure 4: Mean values of the UTCI in winter (DJF, top) and summer (JJA, bottom) in the control period (ctrl) and projection period (proj) as well as the difference (diff) based on the bias-corrected ensemble mean. Changes that are not significant or consistent within the ensemble are dotted.

on hourly values. In the control period, strong heat stress occurs at most on 44 days in southwest Germany. On the Lower Rhine and in eastern Germany, about 30 days are reached. Very strong heat stress occurs most often in the Upper Rhine valley with a maximum of about 5 days in the control period. In northern Saxony as well as parts of Saxony-Anhalt and Brandenburg there can be up to 4 days with very strong heat stress. In the low range mountains as well as at the North Sea and the Baltic Sea very strong heat stress does not occur. The number of days with at least strong heat stress is increasing especially in the southern half of Germany, as well as in northern Saxony, parts of Saxony-Anhalt and Brandenburg. With a maximum of about 20 days, the increase in the southwest corresponds to almost half as many days as in the control period, which means an increase of almost 50 %. Altogether there is a maximum of about 60 days in the year with strong heat stress in the southwest of Germany. An increase of the days with very strong heat stress is projected in particular for the Upper Rhine valley, where the number of days partially more than doubles with an increase of 6 to 9 to about 10 to 15 days. Except for small areas in the mountainous areas of the low range mountains, where very strong heat stress does not occur during the projection period, the changes have an EC of 100 % and a significance at the 95 % level throughout the entire investigation area.

As the number of heat stress events increase, so does the time span from the first to the last occurrence in the year. Figure 6 shows the period between the first and last occurrence of at least moderate and strong heat stress events. In southern Germany, the maximum value in the control period is about 224 days with heat stress and 140 days with strong heat stress. For the North Sea and the Baltic Sea, the period in which heat stress occurs is about 130–140 days on average, which is the same span as the period in which at least strong heat stress occurs in southern Germany. In the projection period, the occurrence of at least moderate respectively strong heat stress events increase to 236 respectively 157 days in south-

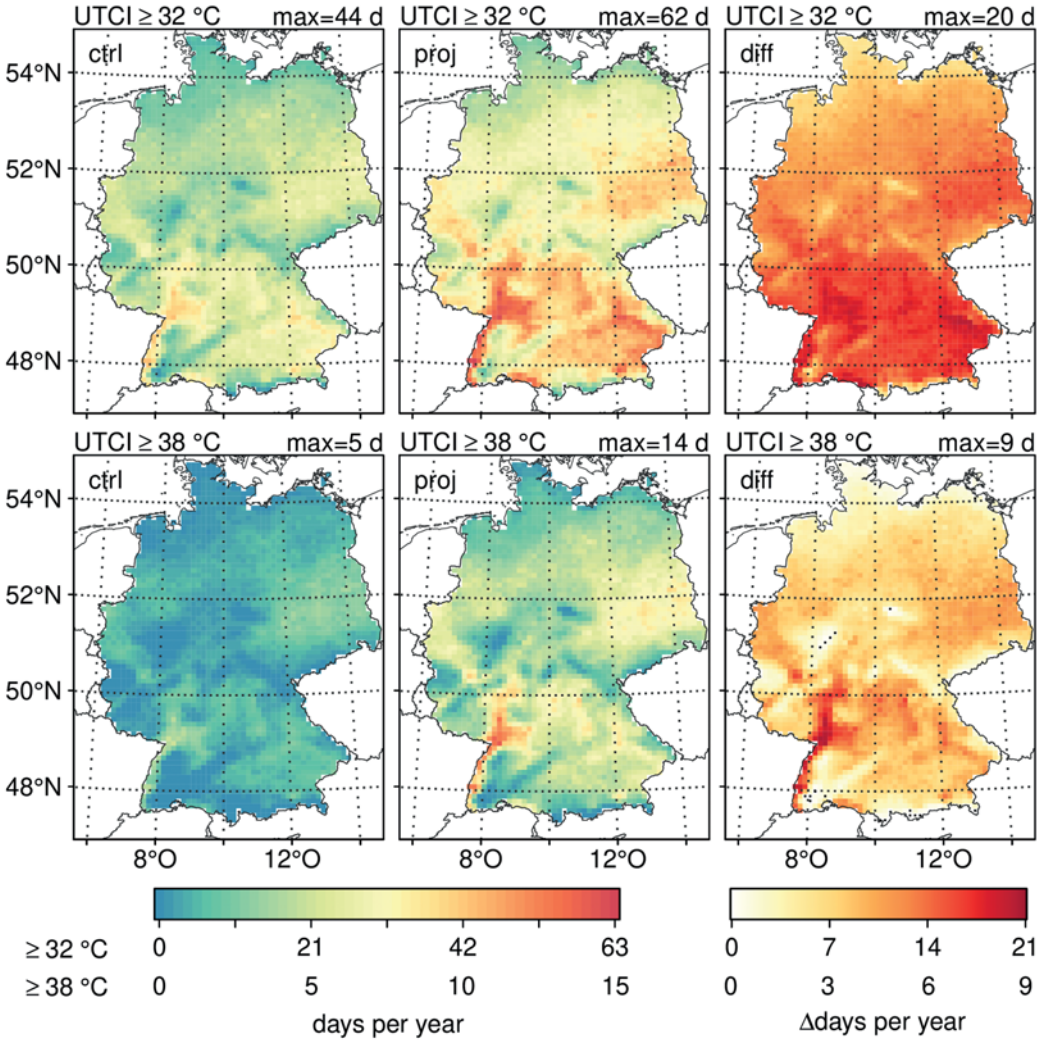

Figure 5: Average number of days (d) per year with the UTCI maximum greater than or equal to 32 °C (top) and 38 °C (bottom) in the control period (ctrl) and projection period (proj) and their difference (diff) based on the bias corrected ensemble mean. Changes that are not significant or consistent within the ensemble are dotted.

ern Germany. On average, the period of occurrence of heat stress events is extended by 14–15 days. Most of the changes are consistent in the ensemble and significant at the 95 % level.

Figure 7 shows the maximum contiguous periods in which at least strong and very strong heat stress occurs. This means that the daily maximum of the respective thermal stress class must be reached at least at one hour per day. For at least strong heat stress the maximum value is 9 days in the southwest, for at least very strong heat stress it is still about 3 days. For the projection period the duration of strong heat stress is projected to be 10–13 consecutive days in the Rhine valley, the Rhine-Neckar area, parts of Saxony, Brandenburg and Saxony-Anhalt, and parts of the Main and Danube valleys, representing an increase of about one third in comparison to the control period. The strongest increases occur in the Danube valley and in the Rhine-Neckar area. EC is 100 % nearly everywhere, significance is at the 95 % level throughout the entire area. Very strong heat stress is reached in the projection period with a maximum of about 7 consecutive days in the Upper Rhine valley and Rhine-Neckar area, almost doubling the mean duration of this heat stress class. Significance at the 95 % level and an EC greater equal 75 % is only reached in the Upper Rhine valley and parts of the remaining Rhine valley, the Rhine-Neckar and Rhine-Main areas, parts of Bavaria, and parts of Saxony, Saxony-Anhalt, and Brandenburg.

The projected changes in the frequency distribution of the UTCI is shown exemplarily in Figure 8 for the city of Mannheim. For the ensemble mean, a shift of the distribution to higher UTCI values with approximately unchanged shape of the distribution can be seen; this is also shown in the results of Cheung and Hart (2014) for Hong Kong. The projected changes in the distribution of the UTCI have a similar shape in all simulations. Due to the shift from stronger and moderate to

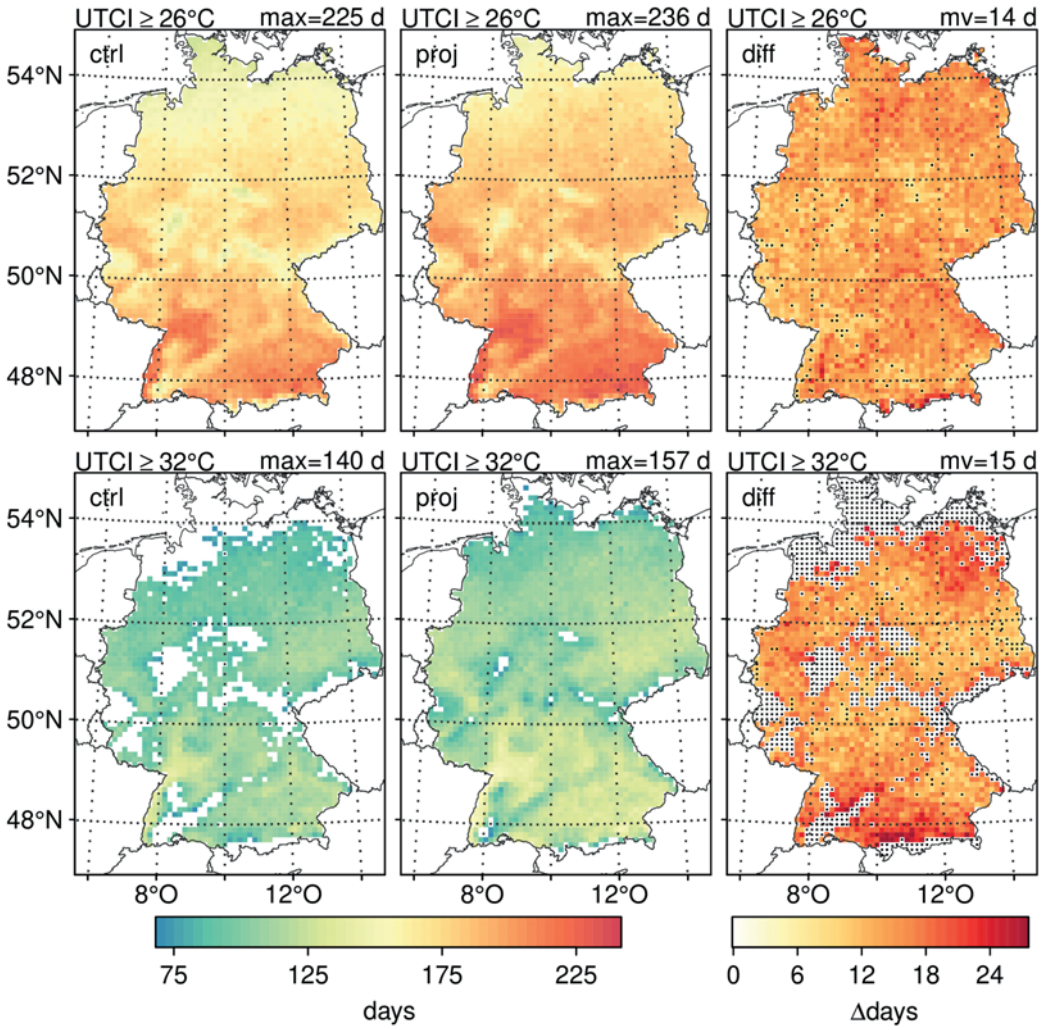

Figure 6: Period between the first and last reaching of the UTCI's at least moderate (26 °C, top) and strong heat stress classes (32 °C, bottom) in the control period (ctrl), projection period (proj) and their difference (diff) in days (d). Values are only displayed where the respective class is reached at least twice each year in the periods shown. Changes that are not significant or consistent within the ensemble are dotted.

slight cold stress and conditions without thermal stress (up to approximately 18 °C UTCI) as well as the shift from slight cold stress and conditions without thermal stress into the thermal comfort range (18 °C to 26 °C UTCI) and to heat stress, the average number of hours with strong and moderate cold stress decrease, whereas the number of hours with slight cold stress and no thermal stress is similar for the control and projection period. On the other hand, the hours in the thermal comfort range and with heat stress increase. In the ensemble mean, heat stress increases by about 230 hours, at least strong heat stress by about 139 hours, and very strong heat stress by about 36 hours per year. The course of the change signal at other locations is similar to that of the site Mannheim. The figure also shows the considerable range of the climate change signal that results from the climate simulations with the same emission scenario, but different GCMs, and highlights the need for ensemble simulations.

3.2 Connection between the UTCI and weather types

In this section we discuss the relation between the UTCI and weather types. For the classification of the weather types we used the method of Bissolli and Dittmann (2001) described in Section 2.7 and the pressure levels suggested therein.

In order to relate the weather conditions and the UTCI, the daily maximum UTCI per grid point for each member of the ensemble is calculated and assigned to the corresponding weather types. The results are then averaged from all individual values at the grid points below 300 m above mean sea level in order to obtain representative heat stress events for the area considered. Although some regions contain more grid points in the study area than others, the results can be assumed to be representative for the whole study area. For grid points

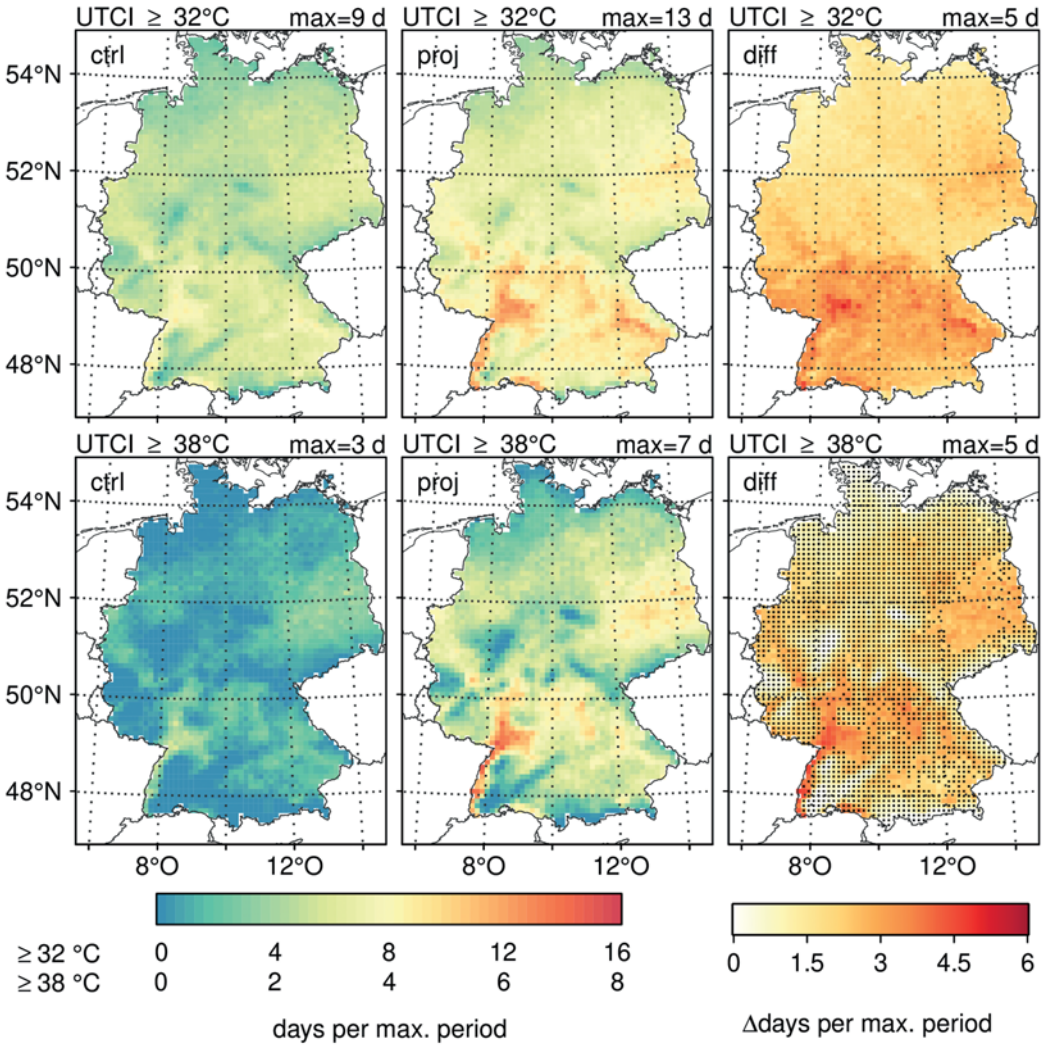

Figure 7: Maximum continuous period in days (d) in the control period (ctrl), projection period (proj) and their difference (diff) in which the daily maxima of the UTCI are not below 32 °C (top) and 38 °C (bottom). Changes that are not significant or consistent within the ensemble are dotted.

above 300 m, the number of heat stress events shifts only to a slightly different level, depending on altitude and geographical location.

We first discuss briefly the current and projected weather type distributions in the investigation area with regard to the criteria advection, cyclonality and humidity. The frequency distribution of the weather types in the control period can be seen e.g. in Bissolli (2003) and Brecht (2019). With regard to advection, the westerly flows (60 %–75 %) dominate, with more northwesterly than southwesterly flow in winter and more southwesterly than northwesterly flow in summer. In all seasons, anticyclonic conditions at ground level dominate (65 % to 75 %). Anticyclonic conditions in 500 hPa also occur more frequently than cyclonic conditions. With regard to humidity in the atmosphere, the data in the control period and the few years shifted period of the reference data set of humidity (1979–1996) show good consistency. The five most common weather types (all year) are, in order of occurence: NWAAD, SWAAW, NWAAW, NWACD und SWCAW.

The projected changes of weather types with respect to the wind direction at 700 hPa show no significant changes for all seasons and with respect to cyclonality at the 950 hPa and 500 hPa levels in winter and autumn. In spring, significant and ensemble consistent changes are projected with an increase of about 2 days of cyclonality at 500 hPa, suggesting more variable weather. For summer, an increase of about 3–4 days of anticyclonic weather types in 500 hPa are projected. From this, more or longer periods of sunny weather for Central Europe can be expected for future summers. This would lead to higher temperature and longer warm periods and could increase heat stress. All climate simulations used here agree in the significant increase of the moisture in the atmosphere between 950 hPa and 300 hPa by 10–20 days per season, probably caused by the increase of the air temperature (Clausius-Clapeyron law).

Figure 9 shows the mean maximum UTCI values in summer depending on the weather type classes of advection and cyclonality for the control period (1981–2000, black) and projection period (2031–2050, red). The

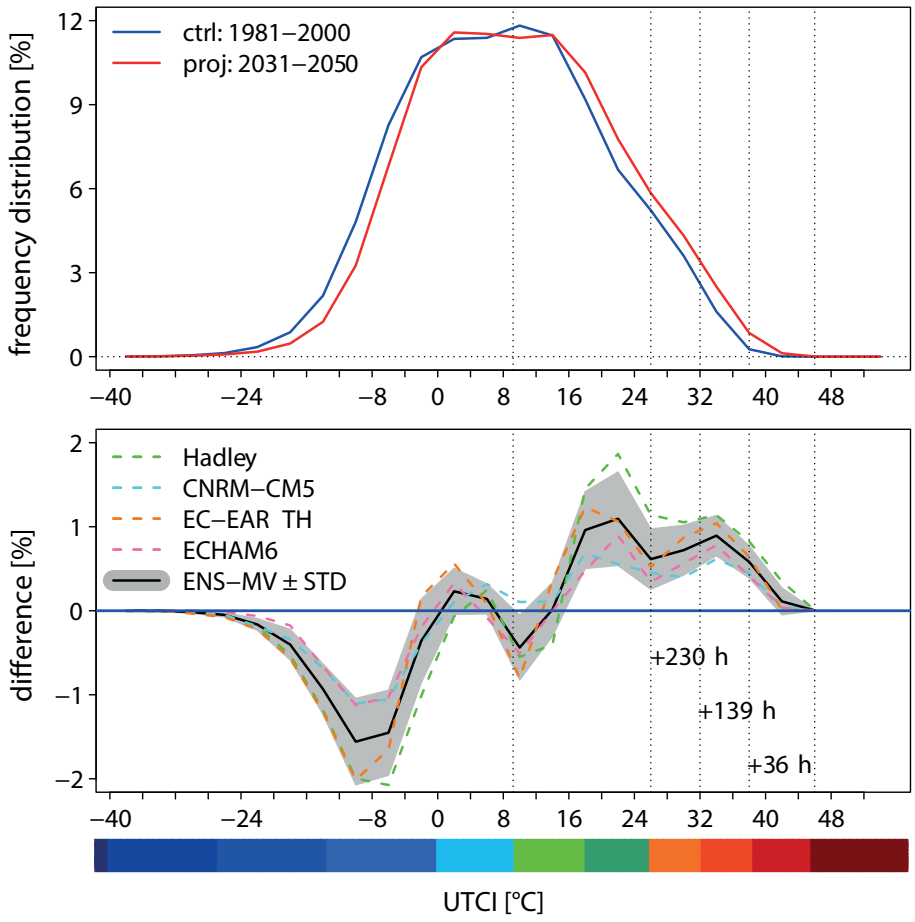

Figure 8: Hourly frequency distribution of the UTCI using the ensemble mean (ENS-MV) for the location Mannheim in 4 K intervals in the control and projection period (top) and difference between projection and control period (bottom). The color scale is associated to the UTCI threshold values of the standard assessment scale given in Table 2.

highest UTCI values occur in the control period with approximately 31 °C for southeasterly flow, and 27 °C to 28 °C for southwesterly flow and undefined wind direction. The highest UTCI values with respect to cyclonality are achieved with anticyclonality at 500 hPa, whereby just about 29 °C are reached. The climate projections show an increase of the mean maximum UTCI for each class of advection and cyclonality in summer. The increases of the mean UTCI with respect to advection is highest for the weather types SW and NW with 2 K. With regard to cyclonality, the changes are greatest with about 2.2 K for anticyclonic weather conditions; this results from clear skies and low wind speeds during these weather conditions. When comparing humidity in the atmosphere, dry weather types show a mean UTCI increase of about 1 K and humid weather types of about 2 K. Significantly more moist than dry weather conditions are projected for the future.

Figure 10 shows the number of weather types per summer that cause at least strong heat stress, i.e. with a maximum UTCI of at least 32 °C. The southwesterly weather type, with about 8 days, provides the largest proportion of weather types associated with strong heat stress. Furthermore, approximately half of all southeasterly weather types in summer also result in a UTCI greater than or equal to 32 °C (Brecht, 2019). However, since southeasterly weather types are less frequent than southwesterly weather types, their fraction in the total amount of all weather types that cause at least strong heat stress is quite low. With regard to cyclonality, anticyclonic weather types in 500 hPa with about 15 days lead most frequently to the occurrence of strong heat stress in summer. About every second anticyclonic weather type in 500 hPa leads to at least strong heat stress in summer (Brecht, 2019). With regard to the humidity in the troposphere, the more humid weather conditions cause understandably more days with a UTCI greater than or equal to 32 °C (10 days) than the dry weather conditions (7 days). For all weather types, an increase of the number of days with at least strong heat stress is projected in the future, except for dry weather types due to their decreasing number. The number of days with at least strong heat stress increases by about 7 days with westerly flow (SW and NW). With regard to cyclonality, the number of days with an UTCI greater than or equal to 32 °C increase for anticyclonic weather conditions (about 9 days), since both their number and the mean maximum UTCI increase, and with regard to tropospheric humidity for humid weather conditions (about 9 days) for the same reasons.

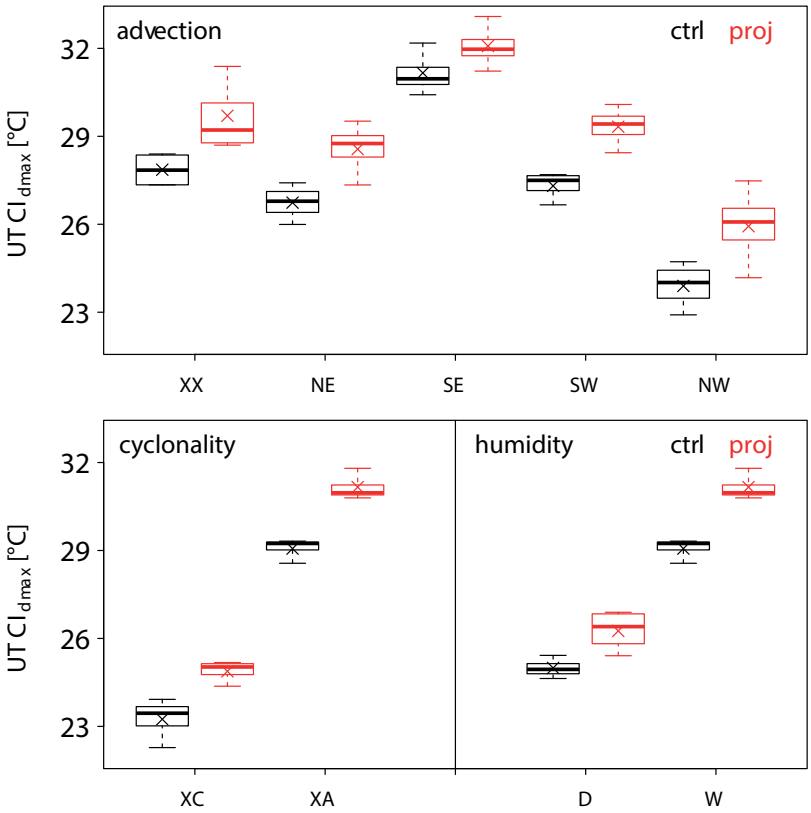

Figure 9: Ensemble mean value (x) from the daily maximum of the UTCI ($UTCI_{dmax}$) depending on the weather type criteria advection (top) and cyclonality as well as humidity in the atmosphere (bottom) in summer (JJA) for the control period 1981–2000 (black) and projection period 2031-2050 (red). In addition to the ensemble mean (x), the box plots represent the 5 %, 25 %, 50 %, 75 % and 95 % percentiles of the ensemble. With regard to advection, XX means undefined main wind direction, NE northeast, SE southeast, SW southwest and NW northwest. With regard to the cyclonality index, XA stands for anticyclonic at 500 hPa and XC for cyclonic conditions at 500 hPa. D stands for dry and W for wet (humid) conditions.

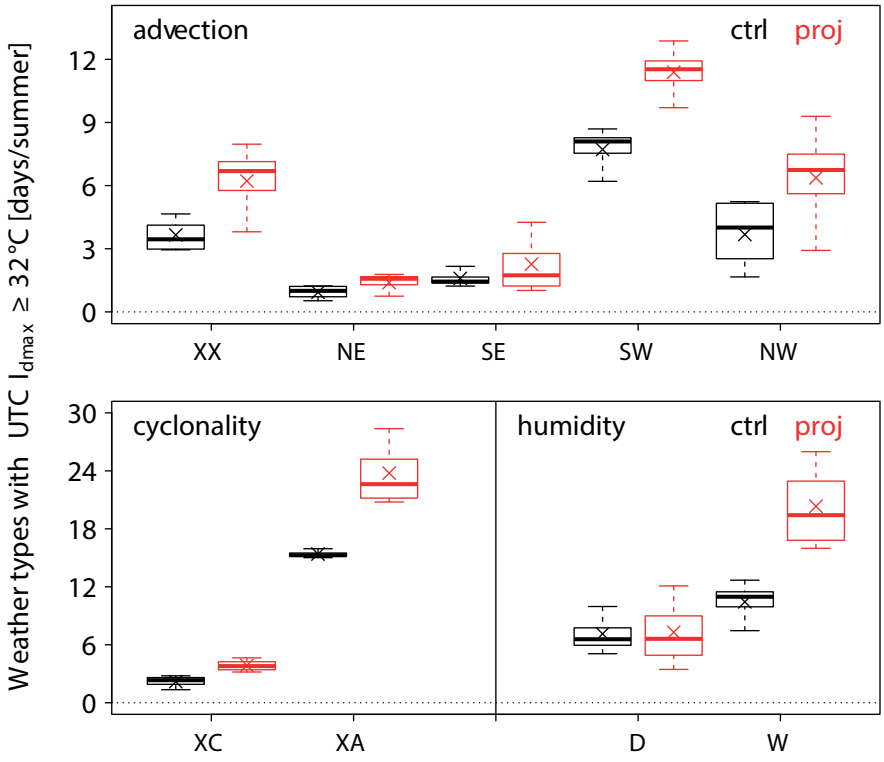

Figure 10: As Figure 9 but for weather types causing at least strong thermal stress (UTCI ≥ 32 °C).

The number of events with strong heat stress in anticyclonic weather types increases from about 15 days to about 24 days in summer, i.e. by about 9 days more in future summers. Also an increase of the anticyclonic weather types of about 3–4 days in summer is projected, as mentioned before. Since not every day with anticyclonic weather causes strong heat stress, about half in the control period and about two thirds in the projecton period in summer (Brecht, 2019), an increase of at most 2–3 days of events with strong heat stress can be assumed due to the increase of anticyclonic weather types. This results in a difference of about 6–7 days with at least strong heat stress events, which cannot be explained by the increase of anticyclonic weather conditions. Therefore, it must rather be concluded that the properties of the atmosphere change towards warmer and more humid conditions. A change in the properties of the atmosphere is also indicated by a significant increase in humid weather conditions by about 18 days per summer. This increase can be explained by the increased capacity of the atmosphere to absorb water due to the increased air temperature in the troposphere (Clausius-Clapeyron law). Throughout the year, there are more humid weather conditions on about 50 days in the projection period compared to the control period. The results are in agreement with those of Sedlmeier (2015), who concludes that the properties of the air masses contribute more to the climate change signal than changes in the frequency of individual weather types; nevertheless, the latter can have an additional effect on the ground-level parameters.

4 Summary and conclusions

We used a small ensemble of regional climate simulations to assess the effect of climate change on heat stress events in Germany. We focused on heat stress, since cold stress can often be reduced to an acceptable level by adaptation, but the possibilities for adaptation to heat stress are limited. Using the regional climate model COSMO-CLM, we downscaled driving data from four GCMs to generate a small ensemble. In order to calculate UTCI thresholds, an hourly bias correction was performed. To preserve the relations between the variables entering the UTCI calculation, the multivariate bias correction method MBCn after Cannon (2017) was applied.

As expected, the regions most affected by heat stress are in southern Germany, especially metropolitan areas in the Rhine valley, and the region south of Berlin (Brandenburg, Lausitz). The climate projections show a significant increase of both the mean UTCI and the number, duration and intensity of heat stress events between the control period (1981–2000) and the projection period (2031–2050). About 50 % more days with strong heat stress (UTCI ≥ 32 °C) and more than twice as many days with very strong heat stress (UTCI ≥ 38 °C) are projected in the future with an ensemble consistency of 100 % for the projected changes. The projected future hourly frequency distribution of the UTCI at a selected location corresponds to a shift to higher UTCI values with an almost unchanged shape of the distribution. Thus, in the future, less hours with cold stress and more hours with heat stress are expected. The spread of the individual ensemble members shows the importance of the ensemble approach with different GCMs as driving data. Although the UTCI thresholds could depend on the region and time period considered, we used the ones given in Bröde et al. (2012) for reasons of comparability and lack of alternative threshold values for future periods; such analyses would go beyond the scope of this study, which focuses on the change in climatologies.

In order to identify the reasons for these future UTCI changes, we looked at possible changes of the relevant weather types and/or changes in the properties of the air masses connected to these weather types; for that purpose, we used the objective weather type classification of the German Weather Service (Dittmann et al., 1995; Bissolli and Dittmann, 2001). No significant changes of the frequency distribution of the weather types between the periods covered were found, with a few exceptions. The most important exception is the increase of summer anticyclonic weather types by 3–4 days per summer. However, the projected increase of heat stress events can be attributed to at most 30 % to the changes of the weather types frequency. Rather, it seems that the characteristics of the atmosphere – i.e. of the air masses – change towards warmer and more humid conditions, which is also indicated by the increasing number of humid weather conditions, i.e. the precipitable water in the troposphere.

In terms of the UTCI, a regionally varying, but everywhere strongly increasing number, duration and strength of heat stress is projected for Germany. Locally, the heat stress events can be even more intense and last longer, especially in cities due to the heat island effect which leads to longer lasting heat stress in the evening and at night compared to surrounding rural areas; this was shown e.g. in Brecht (2019) using CCLM (2.8 km and 925 m mesh size) coupled with the SVAT TERRA_URB (Wouters et al., 2016; Wouters et al., 2017) and in combination with measured data for shorter historical periods using the UTCI. On the microscale, shading plays a major role in the heat stress on sunny days. Inside buildings, the heat stress in summer is usually lower during the day than outside, but higher at night, i.e. assuming natural ventilation of the buildings. With further warming, it will therefore become increasingly difficult to provide thermal comfort in summer at night, especially in cities inside buildings without air conditioning. Therefore, a need for action to protect vulnerable groups in particular from the heat exposure is needed; for that purpose, maps of thermal stress indices like the UTCI can help to identify critical regions and to put into effect adaptation measures. These could contain applying state-of-the-art building technology indoors and outdoors as well as spatial planning, for example. The study

also shows that sustainable protection against increased, longer and more intense heat stress can only be achieved by limiting global warming.

The next steps should include enlarging the ensemble and increasing the model resolution. For planning purposes, the existing ensemble can be used to provide detailed climatologies by coupling building and street resolving urban climate models.

Acknowledgements

This work is funded within the framework of the project "Leistungskriterien für wohnkomfortgerechte Wandbaustoffe unter Einfluss des Klimawandels in Baden-Württemberg" by the Baden-Württemberg foundation, Baden-Württemberg, Germany.

The RCM simulations performed in this study were carried out at the High Performance Computing Center (HLRS) in Stuttgart, Germany.

We also thank the R community for providing the package "MBC" (Cannon, 2017) and its author as well.

We acknowledge support by the KIT-Publication Fund of the Karlsruhe Institute of Technology.

References

Albergel, C., E. Dutra, B. Bonan, Y. Zheng, S. Munier, G. Balsamo, de P. Rosnay, J. Muñoz-Sabater, J.C. Calvet, 2019: Monitoring and forecasting the impact of the 2018 summer heatwave on vegetation. – Remote Sens. **11**, 520.

Arakawa, A., V.R. Lamb, 1977: Computational design of the basic dynamical processes of the ucla general circulation model. – General circulation models of the atmosphere **17**, 173–265.

Bissolli, P., 2003: Objektive Wetterlagenklassen. – Klimastatusbericht des DWD 153–159.

Bissolli, P., E. Dittmann, 2001: The objective weather type classification of the German Weather Service and its possibilities of application to environmental and meteorological investigations. – Meteorol. Z. **10**, 253–260.

Blazejczyk, K., Y. Epstein, G. Jendritzky, H. Staiger, B. Tinz, 2012: Comparison of UTCI to selected thermal indices. – Int. J. Biometeorol. **56**, 515–535.

Brecht, B.M., 2019: Die urbane Wärmebelastung unter Einfluss lokaler Faktoren und zukünftiger Klimaänderungen. – Ph.D. thesis, Institut für Meteorologie und Klimaforschung des KIT.

Bröde, P., D. Fiala, K. Błażejczyk, I. Holmér, G. Jendritzky, B. Kampmann, B. Tinz, G. Havenith, 2012: Deriving the operational procedure for the Universal Thermal Climate Index (UTCI). – Int. J. Biometeorol. **56**, 481–494.

Bürger, G., J. Schulla, A. Werner, 2011: Estimates of future flow, including extremes, of the Columbia River headwaters. – Water Resour. Res. **47**.

Cannon, A.J., 2016: Multivariate bias correction of climate model output: matching marginal distributions and intervariable dependence structure. – J. Climate **29**, 7045–7064.

Cannon, A.J., 2017: Multivariate quantile mapping bias correction: an n-dimensional probability density function transform for climate model simulations of multiple variables. – Climate Dyn. **50**, 31–49.

Chang, E.K., C.G. Ma, C. Zheng, A.M. Yau, 2016: Observed and projected decrease in northern hemisphere extratropical cyclone activity in summer and its impacts on maximum temperature. – Geophys. Res. Lett. **43**, 2200–2208.

Cheung, C.S.C., M.A. Hart, 2014: Climate change and thermal comfort in Hong Kong. – Int. J. Biometeorol. **58**, 137–148.

Collins, W., N. Bellouin, M. Doutriaux-Boucher, N. Gedney, P. Halloran, T. Hinton, J. Hughes, C. Jones, M. Joshi, S. Liddicoat, others, 2011: Development and evaluation of an Earth-System model–HadGEM2. – Geosci. Model Dev. **4**, 1051–1075.

Dee, D.P., S. Uppala, A. Simmons, P. Berrisford, P. Poli, S. Kobayashi, U. Andrae, M. Balmaseda, G. Balsamo, P. Bauer, others, 2011: The ERA-Interim reanalysis: configuration and performance of the data assimilation system. – Quart. J. Roy. Meteor. Soc. **137**, 553–597.

Di Napoli, C., F. Pappenberger, H.L. Cloke, 2018: Assessing heat-related health risk in europe via the universal thermal climate index (utci). – Int. J. biometeorol. **62**, 1155–1165.

Dittmann, E., S. Barth, J. Lang, G. Müller-Westermeier, 1995: Objektive Wetterlagenklassifikation – Selbstverlag des Deutschen Wetterdienstes, Offenbach, 44.

Doms, G., J. Förstner, E. Heise, H.J. Herzog, D. Mironov, M. Raschendorfer, T. Reinhardt, B. Ritter, R. Schrodin, J.P. Schulz, G. Vogel, 2011: A description of the nonhydrostatic regional COSMO-model part II: physical parameterization. – Technical report, http://www.cosmo-model.org/content/model/documentation/core/cosmoPhysParamtr.pdf

Dosio, A., E.M. Fischer, 2018: Will half a degree make a difference? robust projections of indices of mean and extreme climate in europe under 1.5 c, 2 c, and 3 c global warming. – Geophys. Res. Lett. **45**, 935–944.

Fanger, P., 1970: Thermal comfort. Analysis and applications in environmental engineering. – Copenhagen: Danish Technical Press., 244.

Feldmann, H., G. Schädler, H.J. Panitz, C. Kottmeier, 2013: Near future changes of extreme precipitation over complex terrain in Central Europe derived from high resolution RCM ensemble simulations. – Int. J. Climatol. **33**, 1964–1977.

Fiala, D., A. Psikuta, G. Jendritzky, S. Paulke, D.A. Nelson, van W.D. Marken Lichtenbelt, A.J. Frijns, 2010: Physiological modeling for technical, clinical and research applications. – Front. Biosci. **2**, 939–968.

Fiala, D., G. Havenith, P. Bröde, B. Kampmann, G. Jendritzky, 2012: UTCI-Fiala multi-node model of human heat transfer and temperature regulation. – Int. J. Biometeorol. **56**, 429–441.

Fouillet, A., G. Rey, F. Laurent, G. Pavillon, S. Bellec, C. Guihenneuc-Jouyaux, J. Clavel, E. Jougla, D. Hémon, 2006: Excess mortality related to the august 2003 heat wave in france. – International archives of occupational and environmental health **80**, 16–24.

Fragkoulidis, G., V. Wirth, P. Bossmann, A. Fink, 2018: Linking northern hemisphere temperature extremes to rossby wave packets. – Quart. J. Roy. Meteor. Soc. **144**, 553–566.

Frick, C., H. Steiner, A. Mazurkiewicz, U. Riediger, M. Rauthe, T. Reich, A. Gratzki, 2014: Central European high-resolution gridded daily data sets (HYRAS): mean temperature and relative humidity. – Meteorol. Z. **23**, 15–32. DOI: 10.1127/0941-2948/2014/0560.

Gagge, A.P., A.P. Fobelets, L.G. Berglund, 1986: A standard predictive index of human response to the thermal environment. – ASHRAE Tran. **92**, 709–731.

Hackenbruch, J., G. Schaedler, J.W. Schipper, 2016: Added value of high-resolution regional climate simulations for regional impact studies. – Meteorol. Z. **25**, 291–304.

Hackenbruch, J., T. Kunz-Plapp, S. Müller, J.W. Schipper, 2017: Tailoring climate parameters to information needs for local adaptation to climate change. – Climate **5**, 25.

Haldane, J.S., 1905: The influence of high air temperatures no. I. – J. Hyg.-Cambridge **5**, 494–513.

Harlow, F.H., J.E. Welch, 1965: Numerical calculation of time-dependent viscous incompressible flow of fluid with free surface. – The physics of fluids **8**, 2182–2189.

Havenith, G., D. Fiala, K. Błazejczyk, M. Richards, P. Bröde, I. Holmér, H. Rintamaki, Y. Benshabat, G. Jendritzky, 2012: The UTCI-clothing model. – Int. J. Biometeorol. **56**, 461–470.

Hazeleger, W., X. Wang, C. Severijns, S. Ştefănescu, R. Bintanja, A. Sterl, K. Wyser, T. Semmler, S. Yang, Van den B. Hurk, others, 2012: EC-Earth V2.2: description and validation of a new seamless earth system prediction model. – Climate Dyn. **39**, 2611–2629.

Höppe, P., 1999: The physiological equivalent temperature – a universal index for the biometeorological assessment of the thermal environment. – Int. J. Biometeorol. **43**, 71–75.

Im, E.S., J.S. Pal, E.A. Eltahir, 2017: Deadly heat waves projected in the densely populated agricultural regions of South Asia. – Sci. Adv. **3**, e1603322.

IPCC, 2013: Climate change 2013 – the physical science basis: contribution of working group I to the fifth assessment report of the IPCC. – Cambridge University Press, 1535.

IPCC, 2014: IPCC, 2014: climate change 2014: synthesis report. contribution of working groups I, II and III to the Fifth Assessment Report of the intergovernmental panel on Climate Change. IPCC, Geneva, Switzerland **151**.

Jacobsen, I., E. Heise, 1982: A new economic method for the computation of the surface temperature in numerical models. – Beitr. Phys. Atmos. **55**, 128–141.

Jendritzky, G., W. Sönning, H. Swantes, 1979: Ein objektives Bewertungsverfahren zur Beschreibung des thermischen Milieus in der Stadt- und Landschaftsplanung („Klima-Michel-Modell“). – Beitr. d. Akad. f. Raumforschung und Landesplanung Hannover **28**, 85.

Jendritzky, G., G. Menz, H. Schirmer, W. Schmidt-Kessen, 1990: Methodik zur räumlichen Bewertung der thermischen Komponente im Bioklima des Menschen. – Beitr. d. Akad. f. Raumforschung und Landesplanung: Hannover, Germany **114**, 80.

Jendritzky, G., D. Fiala, G. Havenith, C. Koppe, G. Laschewski, H. Staiger, B. Tinz, 2007: Thermische Umweltbedingungen. – Promet **33**, 83–94.

Jendritzky, G., P. Bröde, D. Fiala, G. Havenith, P. Weihs, E. Batchvarova, de R. Dear, 2009: Der thermische Klimaindex UTCI. – Klimastatusbericht des DWD 96–101.

Jendritzky, G., de R. Dear, G. Havenith, 2012: UTCI – Why another thermal index?. – Int. J. Biometeorol. **56**, 421–428.

Kornhuber, K., S. Osprey, D. Coumou, S. Petri, V. Petoukhov, S. Rahmstorf, L. Gray, 2019: Extreme weather events in early summer 2018 connected by a recurrent hemispheric wave-7 pattern. – Env. Res. Lett. **14**, 054002.

Krähenmann, S., A. Walter, S. Brienen, F. Imbery, A. Matzarakis, 2018: High-resolution grids of hourly meteorological variables for Germany. – Theor. Appl. Climatol. **131**, 899–926.

Lau, N.C., M.J. Nath, 2014: Model simulation and projection of european heat waves in present-day and future climates. – J. Climate **27**, 3713–3730.

Liu, X.D., S. Osher, T. Chan, 1994: Weighted essentially non-oscillatory schemes. – J. Comput. Phys. **115**, 200–212.

Lorenz, E.N., 1960: Energy and numerical weather prediction. – Tellus **12**, 364–373.

Lott, F., M.J. Miller, 1997: A new subgrid-scale orographic drag parametrization: Its formulation and testing. – Quart. J. Roy. Meteor. Soc. **123**, 101–127.

Maraun, D., 2013: Bias correction, quantile mapping, and downscaling: revisiting the inflation issue. – J. Climate **26**, 2137–2143.

Matsueda, M., 2011: Predictability of euro-russian blocking in summer of 2010. – Geophys. Res. Lett. **38**.

Mayer, H., P. Höppe, 1987: Thermal comfort of man in different urban environments. – Theor. Appl. Climatol. **38**, 43–49, DOI: 10.1007/BF00866252.

McGregor, G.R., 2012: Universal thermal comfort index (utci). – Int. J. Biometeorol. **56**, 419–419.

Mitchell, D., C. Heaviside, S. Vardoulakis, C. Huntingford, G. Masato, B.P. Guillod, P. Frumhoff, A. Bowery, D. Wallom, M. Allen, 2016: Attributing human mortality during extreme heat waves to anthropogenic climate change. – Env. Res. Lett. **11**, 074006.

Pappenberger, F., G. Jendritzky, H. Staiger, E. Dutra, F. Di Giuseppe, D. Richardson, H. Cloke, 2015: Global forecasting of thermal health hazards: the skill of probabilistic predictions of the universal thermal climate index (utci). – Int. J. Biometeorol. **59**, 311–323.

Rauthe, M., H. Steiner, U. Riediger, A. Mazurkiewicz, A. Gratzki, 2013: A Central European precipitation climatology–part I: generation and validation of a high-resolution gridded daily data set (HYRAS). – Meteorol. Z. **22**, 235–256.

Revich, B., D. Shaposhnikov, 2012: Climate change, heat waves, and cold spells as risk factors for increased mortality in some regions of russia. – Studies on Russian Economic Development **23**, 195–207.

Riediger, U., A. Gratzki, 2014: Future weather types and their influence on mean and extreme climate indices for precipitation and temperature in Central Europe. – Meteorol. Z. **23**, 231–252.

Robine, J.M., S.L.K. Cheung, S. Le Roy, H. Van Oyen, C. Griffiths, J.P. Michel, F.R. Herrmann, 2008: Death toll exceeded 70,000 in europe during the summer of 2003. – Comptes rendus biologies **331**, 171–178.

Rockel, B., A. Will, A. Hense, 2008: The regional climate model COSMO-CLM (CCLM). – Meteorol. Z. **17**, 347–348.

Rummukainen, M., 2010: State-of-the-art with regional climate models. – Wires. Climate Change **1**, 82–96.

Schädler, G., H.J. Panitz, E. Christner, H. Feldmann, M. Karremann, N. Laube, 2018: Regional climate simulations with cosmo-clm: Ensembles, very high resolution and paleoclimate. – In: High Performance Computing in Science and Engineering'17, Springer, 411–429.

Schär, C., 2016: Climate extremes: the worst heat waves to come. – Nat. Climate Change **6**, 128.

Schär, C., G. Jendritzky, 2004: Climate change: hot news from summer 2003. – Nature **432**, 559.

Schipper, J.W., J. Hackenbruch, H.S. Lentink, K. Sedlmeier, 2019: Integrating adaptation expertise into regional climate data analyses through tailored climate parameters. – Meteorol. Z. **28**, 41–57. DOI: 10.1127/metz/2019/0878.

Schubert, S., H. Wang, M. Suarez, 2011: Warm season subseasonal variability and climate extremes in the northern hemisphere: The role of stationary rossby waves. – J. Climate **24**, 4773–4792.

Sedlmeier, K., 2015: Near future changes of compound extreme events from an ensemble of regional climate simulations. – Ph.D. thesis, Institut für Meteorologie und Klimaforschung des KIT.

Sedlmeier, K., H. Feldmann, G. Schädler, 2017: Compound summer temperature and precipitation extremes over central Europe. – Theor. Appl. Climatol. **131**, 1493–1501.

Sherwood, S.C., M. Huber, 2010: An adaptability limit to climate change due to heat stress. – Proc. of the National Academy of Sciences **107**, 9552–9555.

Staiger, H., K. Bucher, G. Jendritzky, 1997: Gefühlte Temperatur. Die physiologisch gerechte Bewertung von Wärmebelastung und Kältestress beim Aufenthalt im Freien in der Maßzahl Grad Celsius. – Ann. Meteorol. **33**, 100–107.

Steppeler, J., G. Doms, U. Schättler, H. Bitzer, A. Gassmann, U. Damrath, G. Gregoric, 2003: Meso-gamma scale forecasts using the nonhydrostatic model LM. – Meteor. Atmos. Phys. **82**, 75–96.

Stevens, B., M. Giorgetta, M. Esch, T. Mauritsen, T. Crueger, S. Rast, M. Salzmann, H. Schmidt, J. Bader, K. Block, others, 2013: Atmospheric component of the MPI-M Earth System Model: ECHAM6. – J. Adv. Model. Earth Sys. **5**, 146–172.

Stott, P.A., D.A. Stone, M.R. Allen, 2004: Human contribution to the European heatwave of 2003. – Nature **432**, 610–614.

Tiedtke, M., 1989: A comprehensive mass flux scheme for cumulus parameterization in large-scale models. – Mon. Wea. Rev. **117**, 1779–1800.

Vautard, R., A. Gobiet, S. Sobolowski, E. Kjellström, A. Stegehuis, P. Watkiss, T. Mendlik, O. Landgren, G. Nikulin, C. Teichmann, others, 2014: The european climate under a 2 c global warming. – Env. Res. Lett. **9**, 034006.

Vernon, H.M., C.G. Warner, 1932: The influence of the humidity of the air on capacity for work at high temperatures. – J. Hyg.-Cambridge **32**, 431–462.

Voldoire, A., E. Sanchez-Gomez, y D.S. Mélia, B. Decharme, C. Cassou, S. Sénési, S. Valcke, I. Beau, A. Alias, M. Chevallier, others, 2013: The CNRM-CM5.1 global climate model: description and basic evaluation. – Climate Dynam. **40**, 2091–2121.

Vrac, M., P. Friederichs, 2015: Multivariate–intervariable, spatial, and temporal–bias correction. – J. Climate **28**, 218–237.

Vrac, M., T. Noël, R. Vautard, 2016: Bias correction of precipitation through Singularity Stochastic Removal: because occurrences matter. – J. Geophys. Res. Atmos. **121**, 5237–5258.

Wicker, L.J., W.C. Skamarock, 2002: Time-splitting methods for elastic models using forward time schemes. – Mon. Wea. Rev. **130**, 2088–2097.

Wouters, H., M. Demuzere, U. Blahak, K. Fortuniak, B. Maiheu, J. Camps, D. Tielemans, van N.P. Lipzig, 2016: The efficient urban canopy dependency parametrization (SURY) v1.0 for atmospheric modelling: description and application with the COSMO-CLM model for a Belgian summer. – Geosci. Model Dev. **9**, 3027–3054.

Wouters, H., M. Varentsov, U. Blahak, J.P. Schulz, U. Schättler, E. Bucchignani, M. Demuzere, 2017: User guide for TERRA URB v2.2: the urban-canopy land-surface scheme of the COSMO model. – Technical report, http://www.cosmo-model.org/content/tasks/workGroups/wg3b/docs/terra_urb_user.pdf.